

Dimensionality Reduction Techniques for Subsurface Modeling

Misael M. Morales, Carlos Torres-Verdín, and Michael J. Pyrcz

February 10, 2025

1 Abstract

2 Dimensionality reduction is essential for subsurface modeling, where vast datasets with millions
3 of measurements pose computational challenges. Advanced hardware and algorithms have en-
4 abled automated rock classification, seismic interpretation, and reservoir simulation, yet high-
5 dimensional data remains a bottleneck. Traditional feature selection helps simplify models, but
6 dimensionality reduction techniques are often required for rapid predictions and enhanced inter-
7 pretability. Inspired by computer vision, where images are compressed into meaningful features,
8 subsurface modeling benefits from encoding techniques that extract latent representations while
9 preserving critical information. This chapter explores popular dimensionality reduction meth-
10 ods, including singular value decomposition (SVD), principal component analysis (PCA), discrete
11 wavelet transform (DWT), dictionary learning (DL), and deep learning-based autoencoders (AE).
12 These techniques optimize storage, reduce computational costs, and improve predictive accu-
13 racy and can be applied to complex workflows such as reservoir simulation, history matching,
14 and geologic modeling. By transforming complex geospatial data into lower-dimensional spaces,
15 they enhance uncertainty quantification and accelerate machine learning workflows. ~~This~~ A chapter
16 provides insights on different dimensionality reduction techniques for subsurface applications, en-
17 suring robust and scalable modeling for energy resource exploration and development.

18
19 **Keywords:** latent space, geologic uncertainty model, spatial data analytics, computer vision

20 Introduction

21 During the last decades, subsurface energy resources have seen immense revolutions with the
22 accelerated developments of hardware and algorithmic technologies to support subsurface modeling
23 [1, 2]. For example, rock classification from core measurements and well logs has been automated
24 using clustering and classification algorithms, while reservoir simulation has seen benefits from

25 rapid proxy models for dynamic predictions [3–6]. In many cases, however, these datasets are
 26 composed of thousands or millions of measurements or grid blocks with tens to hundreds of
 27 features due to the complexity and uncertainty in subsurface models [7–9]. This makes subsurface
 28 modeling a perfect candidate for dimensionality reduction techniques, where hidden patterns and
 29 relationships in data can be simplified into lower-dimensional representations for more robust
 30 predictions and more interpretable models.

31 Supervised machine learning methods, both for regression and classification, can face significant
 32 challenges when dealing with large subsurface datasets [10, 11]. Several techniques for feature
 33 engineering, feature importance, and regularization have been proposed to intelligently reduce
 34 problems with a large number of variables to the key ~~variables~~^A that have the most effect on the
 35 target variable [12, 13]. However, for cases such as reservoir modeling, seismic modeling, and
 36 well log interpretation, a single realization in an uncertainty model can have a large number of
 37 features, making dimensionality reduction crucial for rapid machine learning predictions [14–16].
 38 This is a classical problem in the field of computer vision, where a single image can have upward of
 39 thousands or millions of pixels, and a single label must be extracted. For subsurface modeling, this
 40 translates into interpreting ~~a subsurface~~^A uncertainty model, for example, a multivariate ensemble
 41 of subsurface properties (e.g., porosity, permeability, brittleness, total organic content, acoustic
 42 impedance) to estimate the recoverable resources in place^A, or a large 2D or 3D geologic uncertainty
 43 model of heterogeneous properties (e.g., porosity, permeability) that can be compressed into a
 44 lower-dimensional representation [17, 18].

45 The main idea behind dimensionality reduction techniques is to compress a dataset, X , into a
 46 latent representation that retains the majority of the patterns and details in the data, also known
 47 as *encoding*, such that,

$$z = enc(X) \quad (1)$$

48 where z is the latent representation of X . A mirroring operator of the Encoder, namely the
 49 Decoder, decompresses the latent representation back to the original data space, namely,

$$X' = dec(enc(X)) = dec(z). \quad (2)$$

50 The goal is then to minimize the difference between X and X' , such that $X \approx X'$, by selecting
 51 an optimal latent dimension that allows for reduced multicollinearity, reduced storage, and ac-
 52 celerated processing while still retaining the majority of important features in the data [19, 20].
 53 Performing computationally expensive routines, such as reservoir simulation or history matching,
 54 with the latent representation instead of the full data space now becomes significantly less compu-
 55 tationally expensive and memory intensive, saving computational time and, with the right choice
 56 of dimensionality reduction algorithm and latent dimension, sufficiently accurate [21, 22].

57 To support the valuable adoption of dimensionality reduction in subsurface modeling, this
 58 chapter will focus on the application of several data-driven dimensionality reduction techniques for
 59 subsurface modeling, including singular value decomposition (SVD), principal component analysis
 60 (PCA), discrete wavelet transform (DWT), dictionary learning (DL), and deep learning-based
 61 AutoEncoders (AE).

62 Dataset

63 To demonstrate the application of different dimensionality reduction techniques in subsurface
64 modeling, a synthetic geologic uncertainty model is used. The dataset consists of an ensemble
65 of Gaussian-distributed log-permeability values simulated using Sequential Gaussian Simulation
66 (SGSIM) in SGem [23–25]. The values range from 0.69×10^{-3} mD to 6.77×10^3 mD. A spherical
67 variogram is used with major and minor values of 90 and 30, respectively. A total of 500 realizations
68 are simulated with a resolution of 128×128 for a total of 16,384 parameters. Figure 1 shows the
69 first 15 realizations in the geologic uncertainty ensemble.

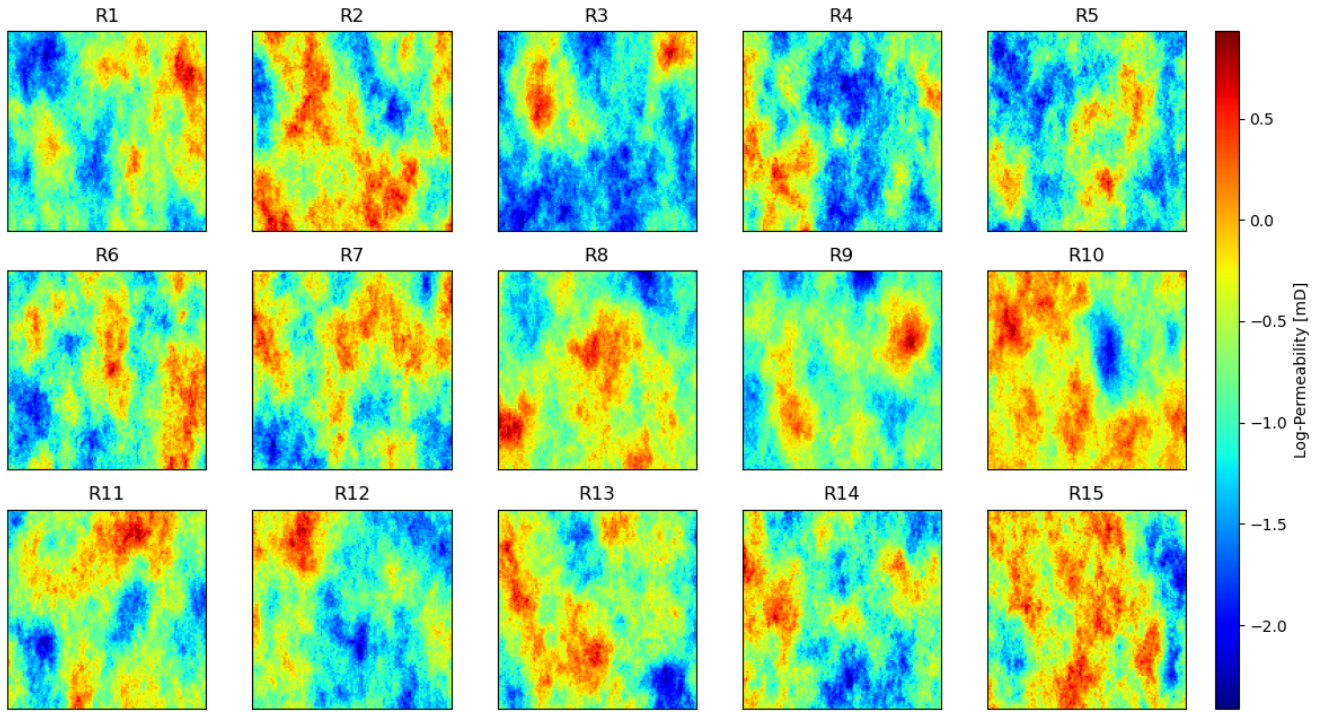


Figure 1: First 15 realizations of the geologic uncertainty model depicting log-permeability values.

70 Singular Value Decomposition

71 The singular value decomposition (SVD) is among the most important matrix factorization algorithms of the computing and provides a numerically stable matrix decomposition useful for a wide
 72 variety of purposes and applications [26, 27]. Moreover, SVD serves as the underlying algorithm
 73 of principal component analysis (PCA), another significant algorithm for dimensionality reduction
 74 [28, 29]. While some dimensionality reduction algorithms provide a generic basis for latent, or
 75 hidden low-dimensional representations, such as the fast Fourier transform (FFT) and the discrete
 76 wavelet transform (DWT), SVD provides a tailored basis. Tailored basis are extracted directly
 77 from the data matrix such that dominant patterns in the data are expressed purely from data,
 78 without the addition of expert knowledge or prior information, while generic basis use predeter-
 79 mined functions, such as sines and cosines, to describe the dominant patterns in the data [30, 31].
 80 Furthermore, SVD is proved to exist for all matrices unlike other transformations such as the
 81 eigendecomposition, making it flexible and versatile any dataset.

82 For subsurface applications, we will focus on image processing or computer vision applications,
 83 where a reservoir model can be described as a matrix with each entry representing a grid block
 84 value of a subsurface property, similar to pixels in an image. Let X be our data matrix such that
 85 $X \in \mathbb{R}^{n \times m}$ is expressed as,

$$X = \begin{bmatrix} | & | & & | \\ x_1 & x_2 & \dots & x_m \\ | & | & & | \end{bmatrix}, \quad (3)$$

86 where each column of X represents a realization of a subsurface uncertainty model, where each
 87 realization $x_k \in \mathbb{R}^n$ has n entries representing each pixel or grid block in the model. Often, the
 88 number of entries, n , (tens of thousands or millions) is much larger than the number of realization,
 89 m (hundreds or thousands).

90 The SVD is a matrix decomposition of X such that,

$$X = U\Sigma V^T, \quad (4)$$

91 where $U \in \mathbb{R}^{n \times n}$ and $V \in \mathbb{R}^{m \times m}$ are unitary matrices with orthonormal columns, and $\Sigma \in \mathbb{R}^{n \times m}$
 92 is a real non-negative diagonal matrix. The columns of U are called the *left-singular vectors* of X
 93 and the rows of V^T are the *right-singular vectors* of X . The diagonal entries of Σ are called the
 94 *singular values* of X and are ordered by magnitude such that the rows and columns of U and V^T
 95 represent the strength of importance of the data matrix X . Finally, the rank of X is equal to the
 96 number of nonzero singular values in Σ .

97 In the case of $m \leq n$, Σ has at most m nonzero elements in the diagonal and can be expressed
 98 as,

$$\Sigma = \begin{bmatrix} \hat{\Sigma} \\ 0 \end{bmatrix}, \quad (5)$$

¹⁰⁰ where $\hat{\Sigma}$ is the nonzero portion of Σ . Thus, we can obtain a lower-dimensional representation of
¹⁰¹ X using the so-called *economy SVD*,

$$X = U\Sigma V^T = [\hat{U} \quad \hat{U}^\perp] \begin{bmatrix} \hat{\Sigma} \\ 0 \end{bmatrix} V^T, \quad (6)$$

¹⁰² where the columns of \hat{U}^\perp span a complementary and orthogonal vector space of \hat{U} .

¹⁰³ In the case of a full-rank Σ , the lower-dimensional representation of X can be obtained by
¹⁰⁴ truncation of the SVD. Here, the matrices \tilde{U} , $\tilde{\Sigma}$, and \tilde{V}^T represent the truncated versions of the
¹⁰⁵ original decomposition matrices up to a chosen singular value such that,

$$X \approx \tilde{U}\tilde{\Sigma}\tilde{V}^T. \quad (7)$$

¹⁰⁶ If X is not full-rank, then some singular values of Σ may still be zero and the truncated SVD
¹⁰⁷ will be exact. However, for truncation values, r , smaller than the rank of X (or the number of
¹⁰⁸ singular values in Σ), there are several ways to optimally select r [32]. One such way is the Scree
¹⁰⁹ plot, or an elbow plot, of the number of singular values retained against the cumulative sum of
¹¹⁰ the singular values, known as *energy*. Once a truncation value r is optimally selected, retaining
¹¹¹ only the leading rows and columns of U , Σ , and V^T will provide an approximate reconstruction
¹¹² of X and a reduced-dimensional representation of the data matrix.

¹¹³ Example

¹¹⁴ To perform SVD, we must vectorize the dataset by making each realization a column vector
¹¹⁵ instead of a matrix, namely $X \in \mathbb{R}^{500 \times 16384}$. Figure 2 shows the leading SVD bases obtained for
¹¹⁶ this dataset. Given that the SVD sorts the leading singular values by magnitude, we observe
¹¹⁷ that the first few bases retain information about the large-scale features in the dataset, while the
¹¹⁸ trailing bases retain fine-scale granular details.

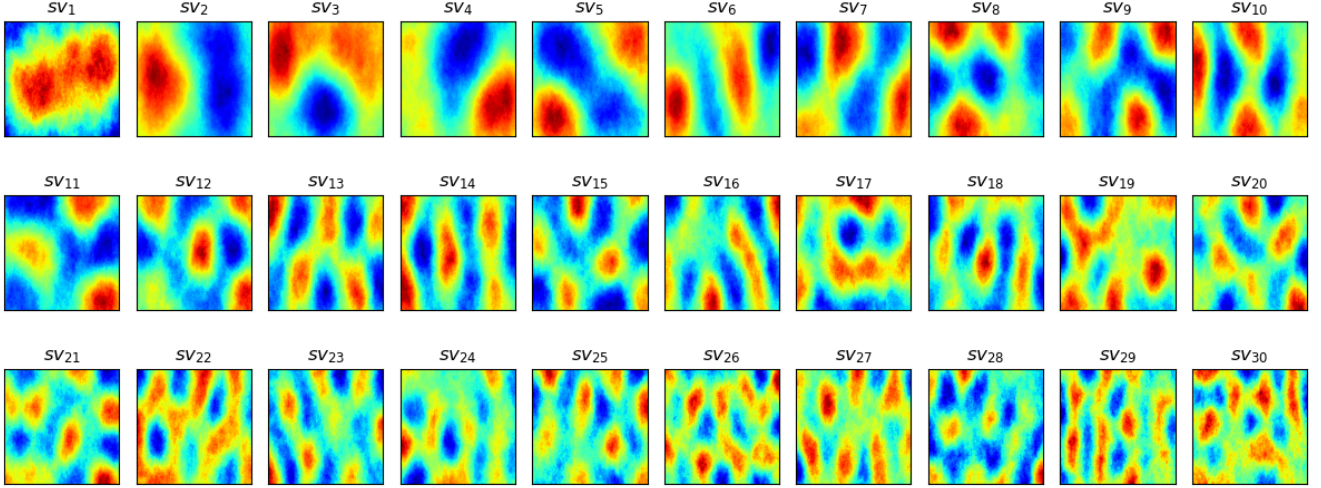


Figure 4 Leading SVD basis for geologic uncertainty dataset.

It is possible to take the SVD of the geologic uncertainty ensemble using different truncation values, r , since $n \leq m$. The Scree plot in Figure 3 shows that by $r = 288$, the singular values account for approximately 80% of the image energy, and by $r = 441$, the singular values account for approximately 95% of the image energy, while $r = 288$ retains approximately 80% of the image energy. Figure 4 show the reconstructed images using k singular values at 20%, 50%, 80% and 95% energy, while Figure 5 shows that using only $k = 441$ singuar values, accouting for 95% of energy retained, we are able to accurately reconstruct the ensemble realizations with an average $R^2=99.27$ and $SSIM=98.83$. The absolute difference between the true and reconstructed images, expressed as,

$$\varepsilon = \left| \frac{X - X'}{X} \right|, \quad (8)$$

shows that the the majority of geologic features and important details are retained, while mostly the noise is filtered out and represented as the error or difference between the images.

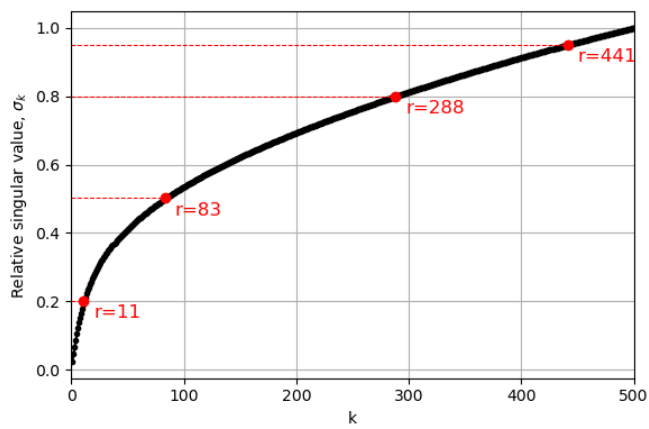


Figure 3: Cumulative energy in the first k singular values.

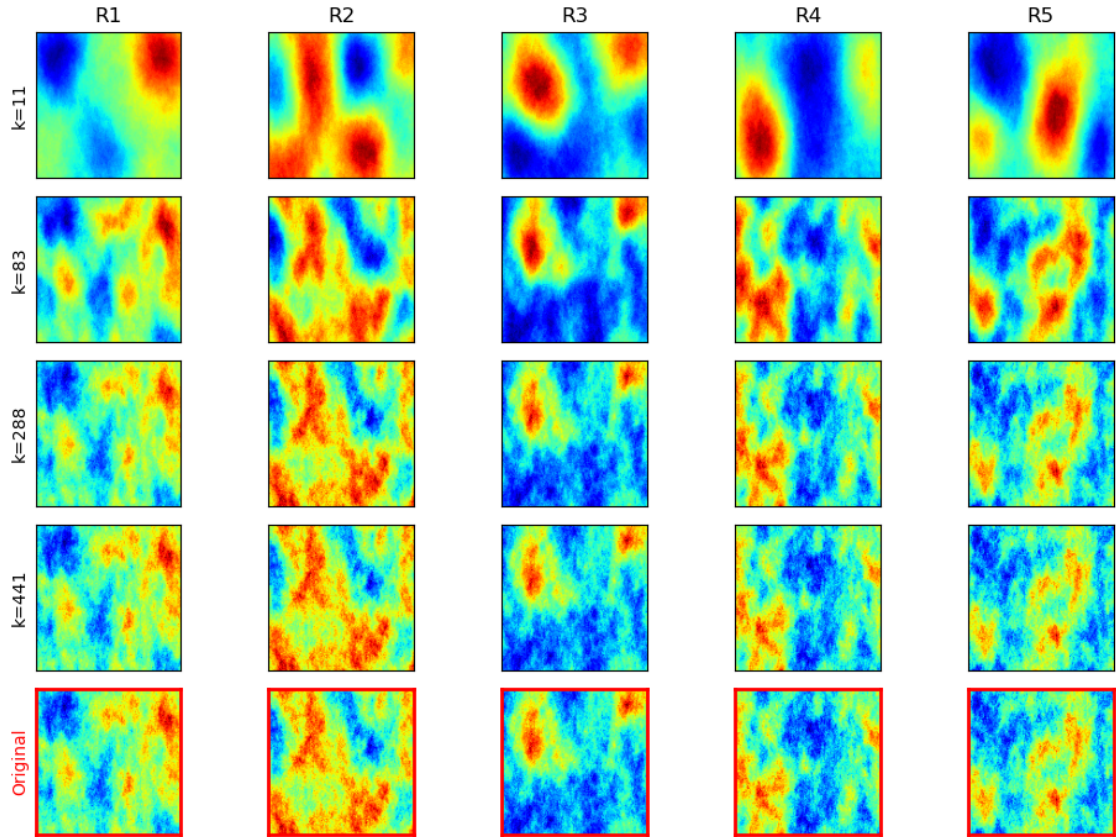


Figure 4: Reconstructed geologic models using k singular values.

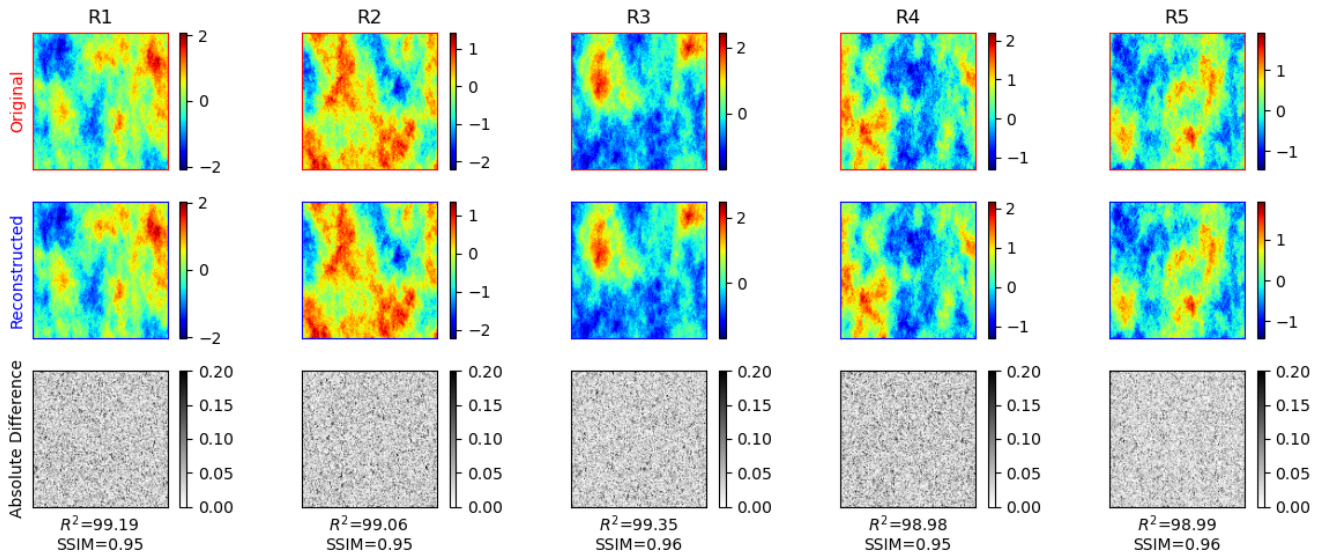


Figure 5: Reconstructed images using $k=441$ singular values accounting for 95% of energy retained.

```

1 import numpy as np                                     # arrays operations
2 from scipy.linalg import svd                         # SVD algorithm
3 from sklearn.metrics import r2_score                 # reconstruction metric
4 from skimage.metrics import structural_similarity    # reconstruction metric
5
6
7 df_perm = np.load('data/data_500_128x128.npy')       # (500, 128, 128)
8 df_perm_f = np.reshape(df_perm, (df_perm.shape[0], -1)) # (500, 16384)
9
10 u, s, vt = svd(df_perm_f.T, full_matrices=True)      # SVD decomposition of X
11 ss = np.diag(s)                                       # diagonalize S
12
13 cutoffs = [0.2, 0.5, 0.8, 0.95]                     # SV energy cutoff values
14 energy = np.cumsum(np.diag(ss))/np.sum(np.diag(ss))   # calculate energy
15 nk = [np.argwhere(energy > cutoff)[0][0] for cutoff in cutoffs] # find truncation indices
16 dd = [u[:, :n] @ ss[:n, :n] @ vt[:n, :] for n in nk]    # truncate based on energy
17 reconstructions = [np.moveaxis(np.reshape(d, (128, 128, -1)), -1, 0) for d in dd]

```

130 Principal Component Analysis

131 Principal component analysis (PCA) is one of the most popular and versatile dimensionality
 132 reduction techniques ~~currently~~, and has been widely applied to subsurface modeling [33–35]. Given
 133 a data matrix $X \in \mathbb{R}^{n \times m}$, PCA aims to find the best linear subspace in the least-squares sense
 134 using the search of rotated orthogonal basis that maximize the variance explained in the first basis
 135 vector, followed by the second orthogonal vector, and so on, as shown in Figure 6 [36, 37]. PCA
 136 preprocesses the data by mean subtraction and setting the variance to unity before performing
 137 SVD, and the resulting coordinate system (principal components) are orthogonal to each other
 138 but have maximum correlation with respect to the data measurements.

139 Let B be the mean subtraction matrix such that,

$$B = X - \bar{X}, \quad (9)$$

140 and the data covariance matrix be given by,

$$C = \frac{1}{n-1} B^T B. \quad (10)$$

141 Then the first principal component is given by,

$$u_1 = \underset{\|u_1\|=1}{\operatorname{argmax}} u_1^T B^T B u_1. \quad (11)$$

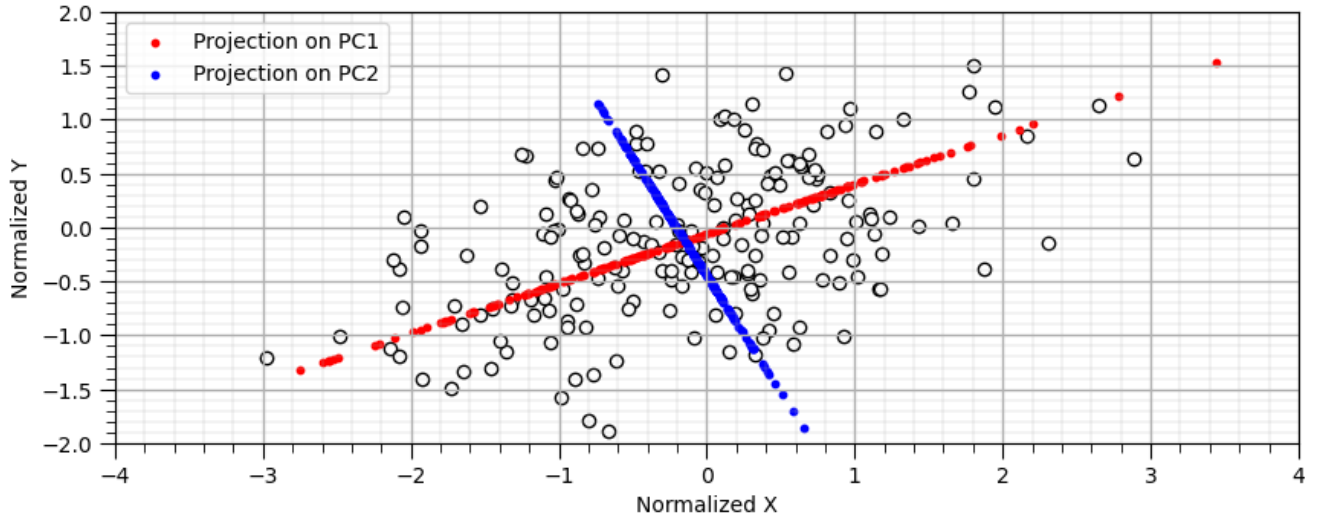


Figure 6: Random multivariate dataset and PCA projection for the first (red) and second (blue) principal components. The PCA projection is the orthogonal rotation to maximize variance explained in the first principal component and remaining variance in the second principal component.

¹⁴² Inherently, u_1 is the first eigenvector of the normalized covariance matrix $B^T B$. The maximum
¹⁴³ number of principal components that can be obtained for a data matrix $X \in \mathbb{R}^{n \times m}$ is given by,

$$\min(m, n - 1), \quad (12)$$

¹⁴⁴ and the remaining principal components can be obtained via de eigendecomposition of C , such
¹⁴⁵ that,

$$CV = VD. \quad (13)$$

¹⁴⁶ PCA converts the set of measurements into a set of linearly uncorrelated features, known
¹⁴⁷ as principal components, which are a linear combination of the original features. The principal
¹⁴⁸ components form a new orthogonal basis, and the principal component scores, or loadings, provide
¹⁴⁹ the linear combination weights. Furthermore, PCA can also be interpreted geometrically as a
¹⁵⁰ matrix rotation, where the original measurements are transformed into a linearly independent
¹⁵¹ subspace of orthogonal vectors, namely the principal components, that maximize the variance
¹⁵² explained. Similar to SVD, the principal components and their corresponding loadings are ordered
¹⁵³ by magnitude, where the leading terms account for the largest possible variance explained [38].

¹⁵⁴ To perform dimensionality reduction on a dataset, we perform truncation and only selecting ~~the~~ k
¹⁵⁵ leading principal components to perform the back-transformation. This ~~will allow~~ us to reconstruct
¹⁵⁶ the back-projected data matrix, X' , by maintaining the principal components with the highest
¹⁵⁷ variance explained while removing the trailing principal components that represent the nuances
¹⁵⁸ or noise in the data.

¹⁵⁹ Example

¹⁶⁰ To perform PCA we must also vectorize the geologic uncertainty dataset by making each realization
¹⁶¹ a column vector instead of a matrix, namely $X \in \mathbb{R}^{500 \times 16384}$. ~~and~~ similar to SVD, PCA sorts the
¹⁶² leading principal components by magnitude. Figure 7 shows the leading components. We observe
¹⁶³ that the first few bases retain information about the large-scale features in the dataset, while the
¹⁶⁴ trailing bases retain fine-scale granular details. Figure 8 shows that with only $r = 234$ PCs, we
¹⁶⁵ are able to retain 95% of the variance explained in the dataset, while using $r = [2, 8, 36]$ retains
¹⁶⁶ 20%, 50%, and 36% of the variance explained in the dataset, respectively.

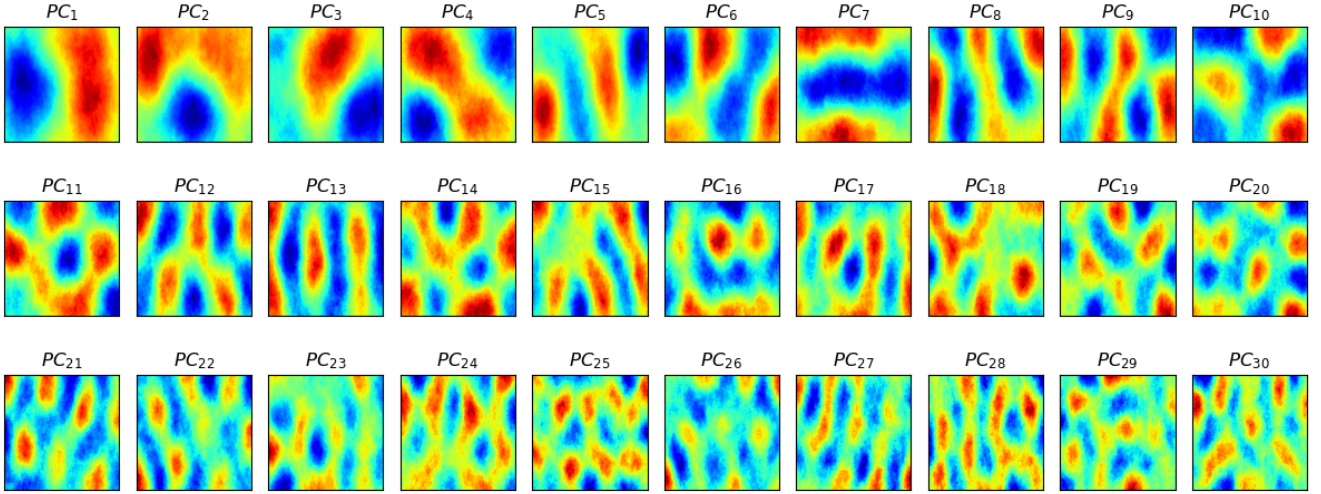


Figure 7: Leading PCA basis for geologic uncertainty dataset.

167 Figure 9 show the reconstructed images using k principal components at 20%, 50%, 80% and
 168 95% variance explained, while Figure 10 shows that using only $k = 234$ principal components,
 169 accounting for 95% of variance explained, we are able to accurately reconstruct the ensemble
 170 realizations with an average $R^2=95.41$ and $SSIM=92.00$.

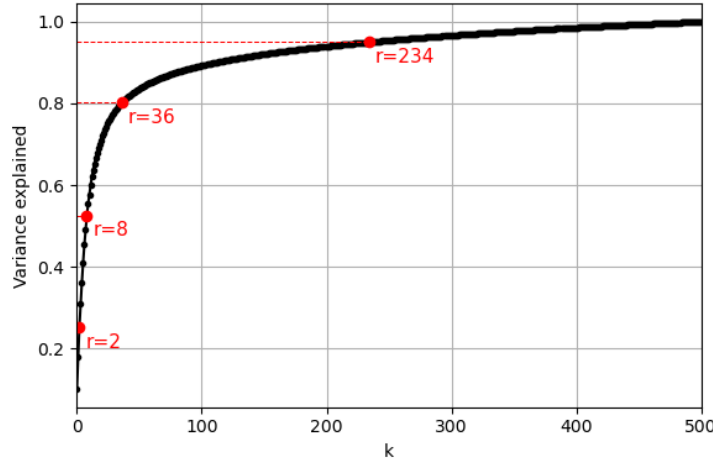


Figure 8: Variance explained against the first k principal components.

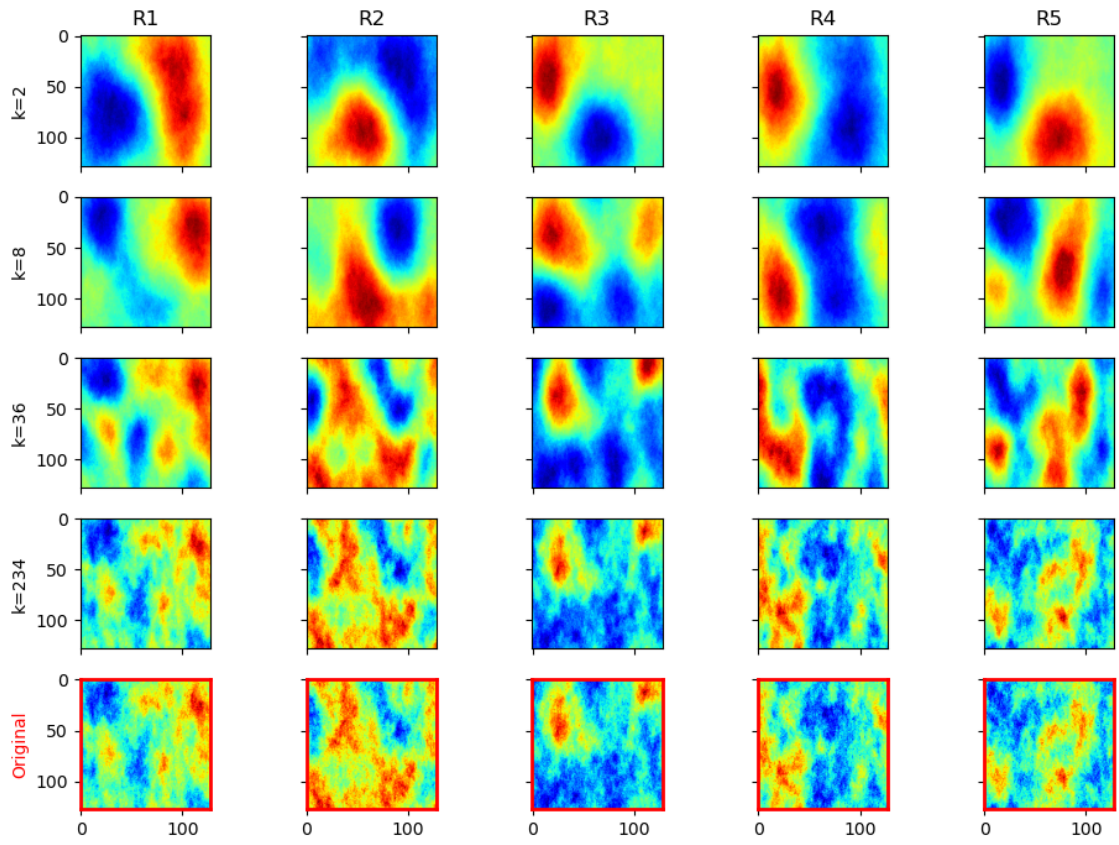


Figure 9: Reconstructed geologic models using k principal components.

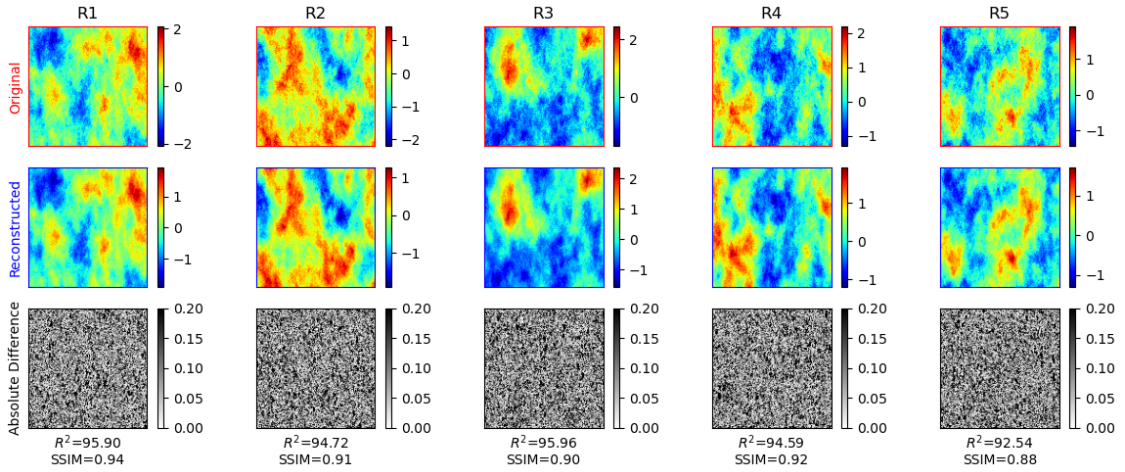


Figure 10: Reconstructed images using $k=234$ principal components accounting for 95% of variance explained.

```

1
2 import numpy as np                                # array operations
3 from sklearn.decomposition import PCA            # PCA algorithm
4 from sklearn.metrics import r2_score             # reconstruction metric
5 from skimage.metrics import structural_similarity # reconstruction metric
6
7 df_perm = np.load('data/data_500_128x128.npy')    # (500, 128, 128)
8 df_perm_f = np.reshape(df_perm, (df_perm.shape[0], -1)) # (500, 16384)
9
10 pca = PCA(n_components=500, svd_solver='full')      # initialize PCA
11 pca.fit(df_perm_f.T)                            # fit PCA to data
12 z = pca.transform(df_perm_f.T)                   # extract PCA latent space
13
14 cutoffs = [0.2, 0.5, 0.8, 0.95]                 # variance explained cutoffs
15 energy = np.cumsum(pca.explained_variance_ratio_) # calculate energy
16 nk = [np.argwhere(energy > cutoff)[0][0] for cutoff in cutoffs] # find truncation indices
17
18 # save latent space and reconstructions for each PCA decomposition level
19 reconstructions = []
20 for i, k in enumerate(nk):
21     pca = PCA(n_components=k)                      # initialize PCA
22     pca.fit(df_perm_f.T)                         # fit PCA to data
23     z = pca.transform(df_perm_f.T)                # extract PCA latent space
24     xhat = pca.inverse_transform(z)               # inverse PCA reconstruction
25     r = np.moveaxis(np.reshape(xhat, (128, 128, -1)), -1, 0) # reshape reconstruction
26     reconstructions.append(r)                    # save reconstructions

```

¹⁷¹ Discrete Wavelet Transform

¹⁷² To explain the discrete wavelet transform, one must first take a look at the Fourier transform.
¹⁷³ The Fourier transform is a central topic in physics and engineering, involving a transformation
¹⁷⁴ of equations into a simple basis to simplify and decouple equations and make computations and
¹⁷⁵ analysis more efficient [39, 40]. The main idea behind the Fourier transform is to decompose a
¹⁷⁶ signal into a set of sine and cosine ~~function~~ with increasing frequencies to provide an orthogonal
¹⁷⁷ basis for the space of solutions to an equation [41]. Unlike SVD and PCA, where the set of
¹⁷⁸ orthogonal ~~basis~~ are *tailored* to the data, the Fourier transform provides a *generic* basis (sines
¹⁷⁹ and cosines) to parameterize any data space into frequency and phase [30].

¹⁸⁰ Mathematically, the Fourier transform is expressed as

$$f(x) = \frac{a_0}{2} + \sum_{k=1}^{\infty} [a_k \cos\left(\frac{k\pi x}{L}\right) + b_k \sin\left(\frac{k\pi x}{L}\right)] = \sum_{k=-\infty}^{\infty} c_k e^{\frac{ik\pi x}{L}}, \quad (14)$$

¹⁸¹ where a_k and b_k are the sine and cosine coefficients, respectively, L is the domain range such that
¹⁸² $x \in [-L, L]$, and k is the frequency.

¹⁸³ Computationally, the Fourier transform of a data matrix can be computed using the Fast
¹⁸⁴ Fourier Transform [42, 43]. This classical algorithm has become ubiquitous in all fields of science
¹⁸⁵ and engineering, allowing for rapid image and audio compression and other ~~application~~. However,
¹⁸⁶ the Fourier transform suffers from localization and loss of resolution, especially in time-frequency
¹⁸⁷ analysis [44]. Wavelets and the Discrete Wavelet transform (DWT) become the candidate solution
¹⁸⁸ for more complex problems.

¹⁸⁹ DWT is based on the Fourier transform, but extends the transformation to a more general
¹⁹⁰ orthogonal basis and ~~exploit~~ multi-resolution decompositions by enabling different time and fre-
¹⁹¹ quency scales, namely the decomposition levels [45, 46]. This is particularly useful for decomposing
¹⁹² complex measurements, especially for image and video decomposition and compression [47]. The
¹⁹³ principal idea behind DWT is to start with a generating function, $\psi(t)$, also known as the *mother*
¹⁹⁴ wavelet, and generate a family of scaled and translated ~~version~~ of the function such that,

$$\psi_{a,b}(t) = \frac{1}{\sqrt{a}} \psi\left(\frac{t-b}{a}\right), \quad (15)$$

¹⁹⁵ where a and b are learnable parameters representing the scale and translation of the function ψ ,
¹⁹⁶ respectively. Typically, the generating wavelet is selected to be an orthogonal function to provide
¹⁹⁷ a hierarchical basis. Therefore, any dataset or function $X = f(t)$ can be described as

$$X = \sum_{i=-\infty}^{\infty} a_k \phi(t) + \sum_{i=-\infty}^{\infty} \sum_{j=0}^{\infty} b_{j,k} \psi(t), \quad (16)$$

¹⁹⁸ where ϕ is a scaling function, ψ is the general wavelet, and a and b are the scaling and translation
¹⁹⁹ parameters, respectively.

200 For a 2D image, a level 1 DWT decomposition divides the data matrix into two discrete
 201 components, namely the approximation and details. A filter bank, or cascading set of high-
 202 pass and low-pass filters, is applied to the data matrix such that the first set obtains a low-pass
 203 horizontal filter (L) and a high-pass horizontal filter (H). Then each sub-image is filtered vertically
 204 using the low-pass and high-pass filter to obtain LL , HL , LH , and HH , respectively, also referred
 205 to as the approximate (A), horizontal (H), vertical (V), and diagonal (D) coefficients. The level
 206 1 DWT coefficient matrix can then be represented as,

$$X = \begin{bmatrix} A & H \\ V & D \end{bmatrix}. \quad (17)$$

207 Example

208 The first step to perform DWT is to select hyperparameters, namely ~~the generating~~^{the} wavelet and
 209 the number of decomposition levels. Here, we will use only 1 decomposition level and the Haar
 210 wavelet, which provides the orthogonal basis needed for the decomposition. Since DWT provides
 211 a multi-resolution orthogonal basis in two-dimensional space, there is no need to vectorize the
 212 data matrix $X \in \mathbb{R}^{500 \times 128 \times 128}$. Figure 11 shows the coefficients in the DWT decomposition for the
 213 first few realizations of our geologic uncertainty model dataset. Figure 12 shows the structural
 214 similarity index measure ($SSIM$) of the reconstructed versus true images in the ensemble as a
 215 function of the percent of DWT coefficients retained.

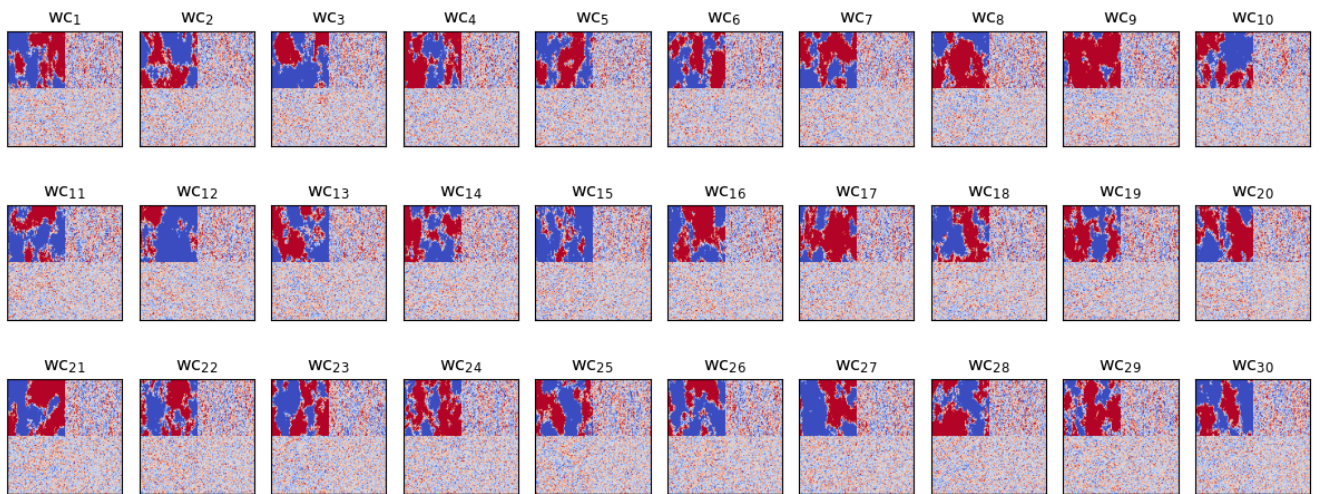


Figure 11: DWT basis for geologic uncertainty dataset. The top left quadrant represents the approximate (A) coefficients, the top right quadrant represents the horizontal coefficients (H), the bottom left quadrant represents the vertical (V) coefficients, and the bottom right quadrant represents the diagonal coefficients (D), as expressed in Eq. 17.

216 To obtain a latent representation of reduced-dimensions from the DWT projection, we must
 217 truncate the trailing coefficients based on their magnitudes. We observe that by retaining only 5%
 218 of the DWT coefficients, we obtain a reconstruction with $SSIM = 46.2$, while retaining 20% of the
 219 DWT coefficients already provide a reconstruction with $SSIM = 94.7$, and retaining 50% of the
 220 DWT coefficients provide an almost lossless reconstruction with $SSIM = 99.36$. Figure 13 shows
 221 the reconstructed images from the geologic uncertainty ensemble using 5%, 20%, 50% and 80%
 222 of DWT coefficients, while Figure 14 shows that using only 50% of the DWT coefficients, we are
 223 able to obtain an accurate reconstruction with $SSIM = 99.36$, $R^2 = 99.26$, and $MSE = 0.027$.

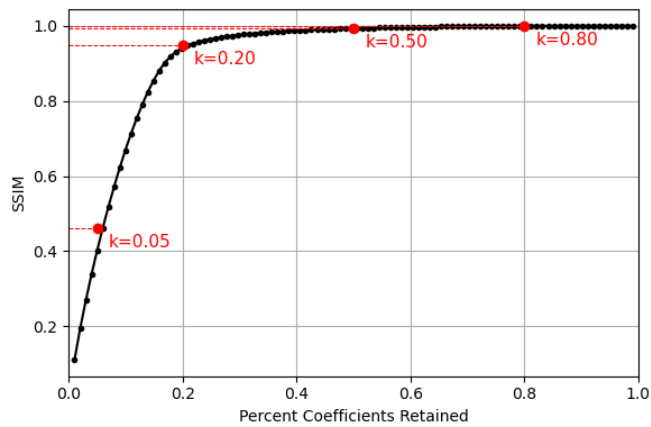


Figure 12: SSIM by number of DWT coefficients retained.

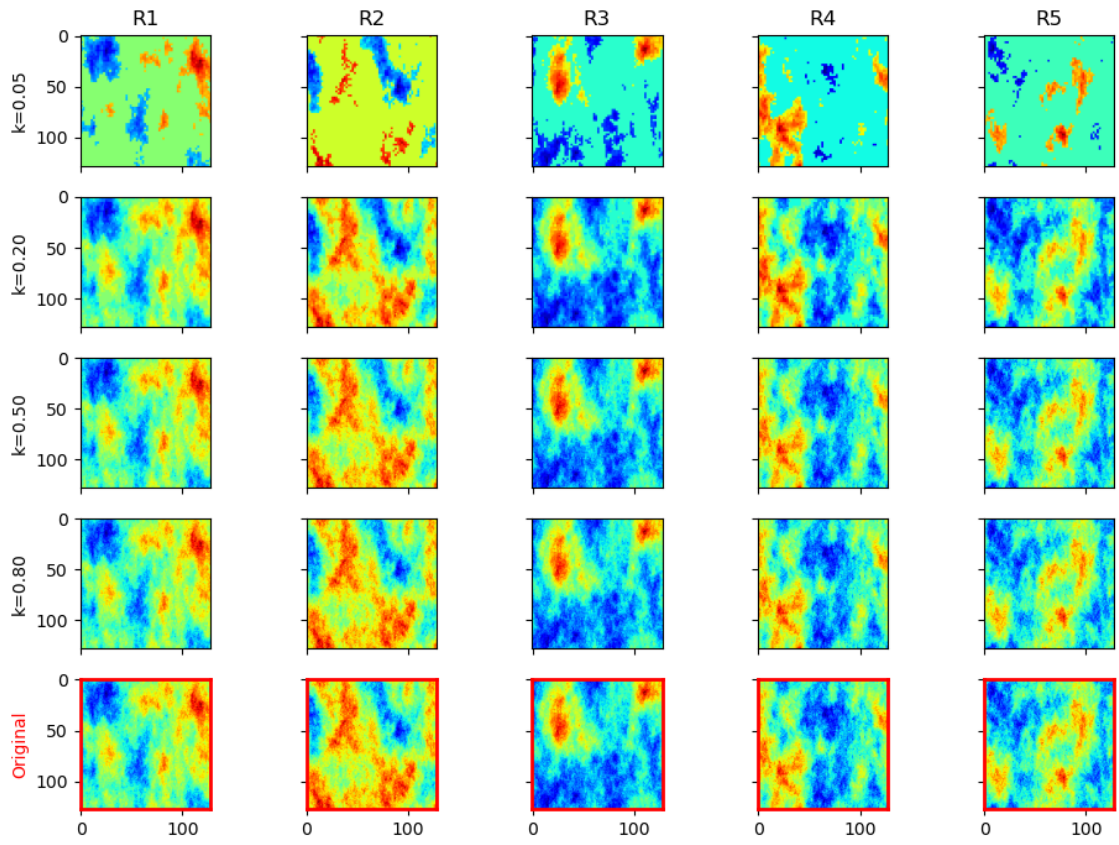


Figure 13: Reconstructed geological models by retaining $k=\{5, 20, 50, 80\}\%$ of DWT coefficients.

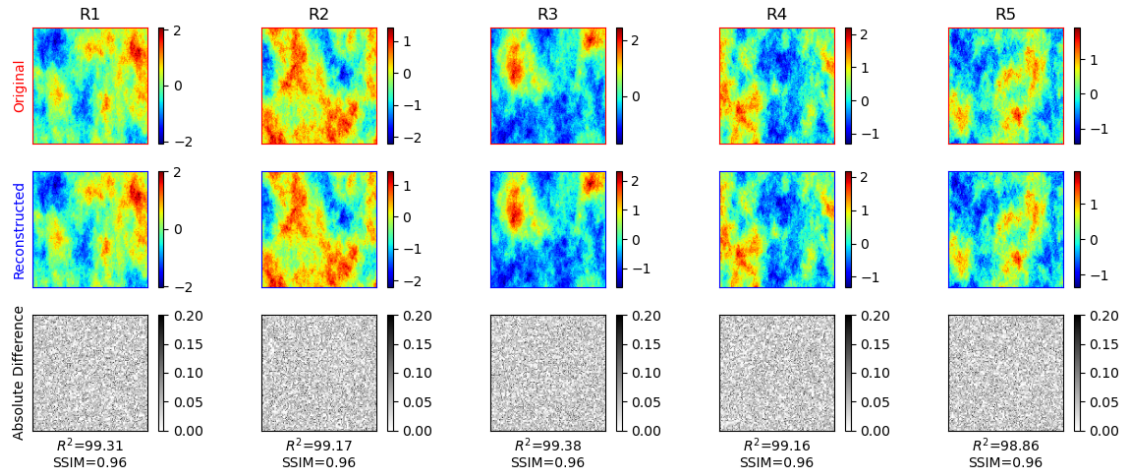


Figure 14: Reconstructed images using $k=50\%$ DWT coefficients accounting for 99% SSIM.

```

1 import numpy as np                                # array operations
2 from pywt import wavedec2, waverec2              # DWT operations
3 from pywt import coeffs_to_array, array_to_coeffs # DWT coefficients-to-arrays
4 from skimage.metrics import structural_similarity # reconstruction metrics
5 from skimage.metrics import peak_signal_noise_ratio # reconstruction metrics
6 from skimage.metrics import mean_squared_error    # reconstruction metrics
7
8 df_perm = np.load('data/data_500_128x128.npy')      # (500, 128, 128)
9
10 keep_percs = np.linspace(0.01, 0.99, 100)          # energy cutoffs
11 wavelet = 'haar'                                    # generating wavelet
12 levels = 1                                         # decomposition level
13
14
15 reconstructions = {'xhat':[], 'coeffs':[]}
16 for i, k in enumerate(keep_percs):
17     c = wavedec2(df_perm, wavelet=wavelet, level=levels) # DWT coefficients
18     c_arr, c_slices = coeffs_to_array(c)                  # coefficients-to-array
19     c_sort = np.sort(np.abs(c_arr.reshape(-1)))           # sort by magnitude
20
21     threshold = c_sort[int(np.floor((1-k)*len(c_sort)))] # cutoff indices
22     c_arr_t = c_arr * (np.abs(c_arr) > threshold)       # truncate coefficients
23     c_t = array_to_coeffs(c_arr_t, c_slices)             # array-to-coefficients
24     recs = waverec2(c_t, wavelet=wavelet)                # reconstructed images
25
26     reconstructions['xhat'].append(recs)                 # store reconstructions
27     reconstructions['coeffs'].append(c_arr)               # store coefficients

```

224 Dictionary Learning

225 Dictionary Learning (DL) is a sparsity-promoting dimensionality reduction method that aims to
 226 find a sparse representation of the data matrix from a linear combination of basic elements [48, 49].
 227 The basic elements, known as *atoms* or *words*, need not to be orthogonal as the *dictionary* of
 228 atoms can be overcomplete (more atoms than realizations) or undercomplete (less atoms than
 229 realizations). For dimensionality reduction purposes, we will focus on undercomplete dictionaries
 230 where the data signal can be represented with a linear combination of a limited number of atoms.

231 Similar to PCA and SVD, dictionary learning provides a *tailored* basis for the data, where
 232 the atoms are not generic but rather learned from the samples directly. DL takes advantage of
 233 the fact that images can often be represented as sparse signals, meaning that a set of images can
 234 be represented as a linear combination of basic images, namely the atoms. The atoms can be
 235 members of the ensemble or new realizations that combine features from the general population.
 236 The data matrix, X , is approximated by the dictionary, D , and the sparse code, S , such that,

$$X \approx DS. \quad (18)$$

237 Because the dictionary is not a unique parameterization, this becomes a minimization problem
 238 such that

$$\begin{aligned} & \text{minimize} && \|X - DS\|_F^2 \\ & \text{subject to} && \|s_i\|_0 \leq K, \\ & && \|d_i\|_2^2 \leq 1 \end{aligned} \quad (19)$$

239 where K is the sparsity level, d_i are the atoms in the dictionary, and $\|\cdot\|_F$ is the Frobenius norm.
 240 However, the ℓ_0 -norm is a non-convex and discontinuous function, making the problem *NP-hard*
 241 and intractable. Therefore, the solution is obtained using a relaxation term, or regularization,
 242 such that the minimization becomes,

$$\min_{D,S} \sum_{i=1}^K \|X - DS\|_F^2 + \lambda \|s_i\|_0. \quad (20)$$

243 This formulation still leads to a sparsity-promoting solution by compressed sensing, given that
 244 S is sufficiently sparse, D is orthonormal, and X contains sufficient measurements [50, 51]. The
 245 choice of the regularization hyperparameter, λ , must also be carefully considered.

246 The most common approach to solve this minimization problem is the k -SVD algorithm,
 247 which is a generalization of the k -Means algorithm with iterative SVD to update the atoms of
 248 dictionary. This two-step solution aims to find the optimal sparse coding, S , followed by updating
 249 the dictionary, D , to encode each element in the data matrix by a linear combination of not more
 250 than K atoms.

251 **Example**

252 Dictionary Learning (DL) is especially useful for dimensionality reduction of image ensembles.
 253 First, we construct a complete dictionary (500 atoms) to observe the sparse representations ob-
 254 tained by DL, as shown in Figure 15. However, since most images can be represented as a linear
 255 combination of sparse signals, we can construct an undercomplete dictionary to parameterize the
 256 data. The atoms in the dictionary are not necessarily ordered by magnitude or energy preserved,
 257 but are altogether a sparse representation of the data matrix. Figure 16 shows *SSIM* of the of
 258 the reconstructed data matrix against the number of atoms in the dictionary used to reconstruct.
 259 We observe that $k = 191$ atoms provide an $SSIM = 0.50$, while using $k = 426$ and $k = 491$ atoms
 260 gives $SSIM = 0.8$ and $SSIM = 0.95$, respectively.

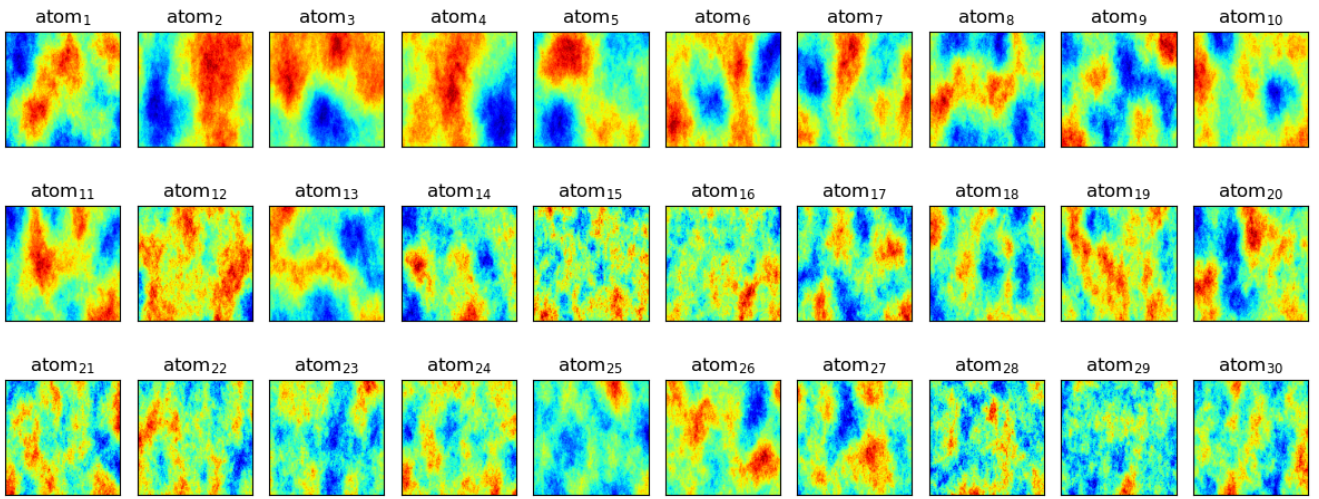


Figure 15: Dictionary atoms for geologic uncertainty dataset.

261 Figure 17 shows the reconstructed image using $k = 16$, $k = 191$, $k = 426$, and $k = 491$
 262 atoms, representing a reconstruction *SSIM* of 0.20, 0.50, 0.80, and 0.95, respectively. We observe
 263 that using only 16 atoms, most reconstructions are not able to reconstruct the patterns in the
 264 first few realizations of the ensemble. However, with 191 atoms, the main patterns in the images
 265 are reconstructed, and with 426 atoms we have almost lossless reconstructions. Figure 18 shows
 266 the true and reconstructed samples using $k = 426$ atoms with an average $SSIM = 0.80$ and
 267 $R^2 = 0.97$.

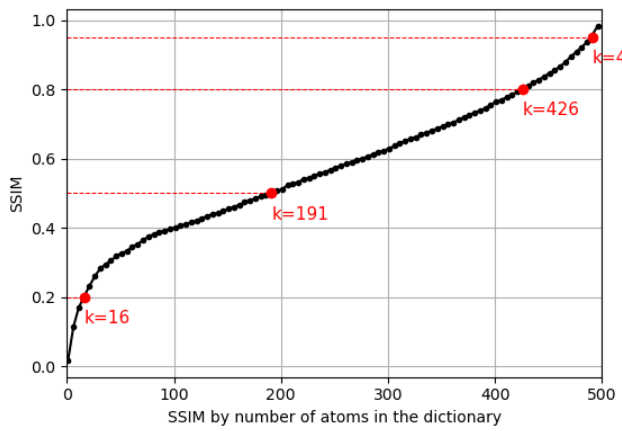


Figure 16: SSIM by number of dictionary atoms retained.

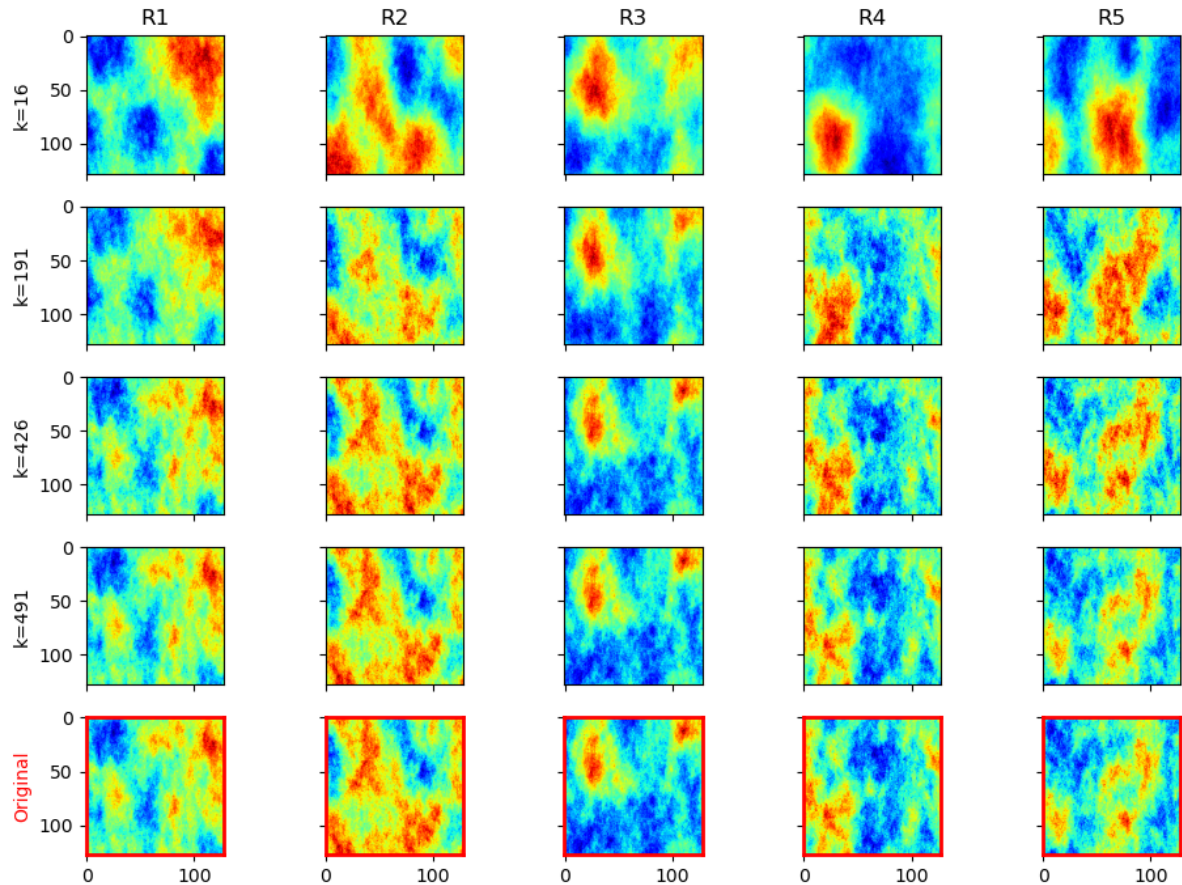


Figure 17: Reconstructed geologic models by retaining k dictionary atoms.

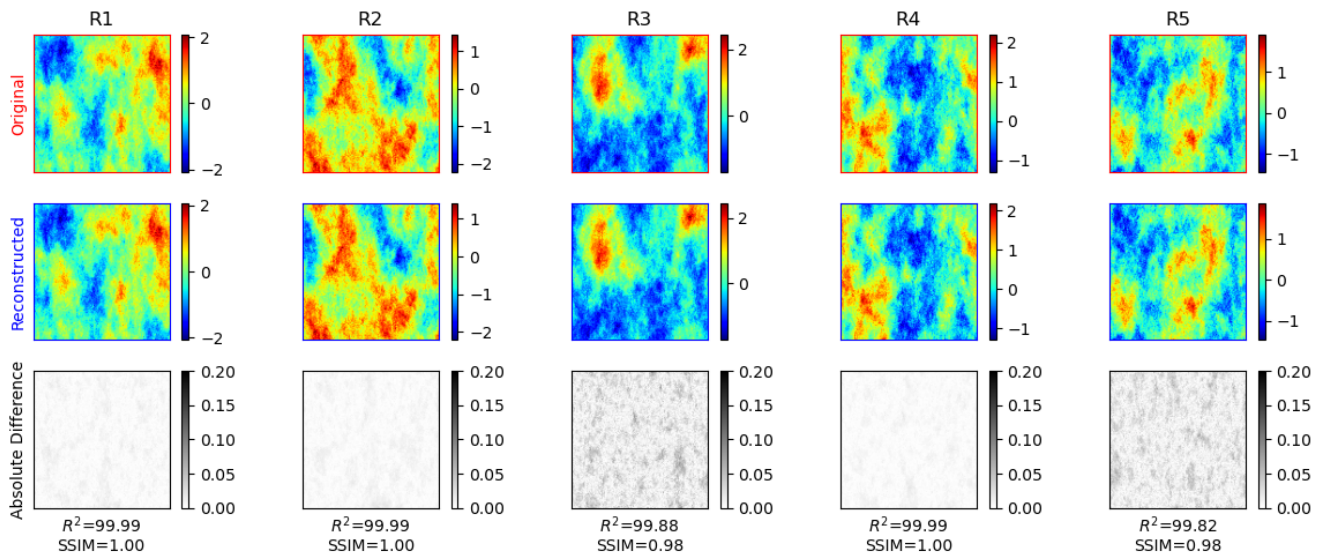


Figure 18: Reconstructed images using $k=426$ dictionary atoms accounting for 80% SSIM.

```

1 import numpy as np                                # array operations
2 from sklearn.decomposition import DictionaryLearning # dictionary learning
3 from sklearn.decomposition import SparseCoder      # sparse coding
4
5 df_perm = np.load('data/data_500_128x128.npy')      # (500, 128, 128)
6 df_perm_f = np.reshape(df_perm, (df_perm.shape[0], -1)) # (500, 16384)
7
8 n_atoms = 500                                     # atoms in dictionary
9 dl = DictionaryLearning(n_components=n_atoms)       # initialize dictionary
10 dictionary = dl.fit(df_perm_f)                   # fit to data matrix
11 atoms = dictionary.components_                  # extract atoms
12
13 sparse_code = SparseCoder(atoms).fit_transform(df_perm_f) # train sparse coder
14 sparse_recs = np.reshape(sparse_code @ atoms, df_perm_f.shape) # reconstructed images
15
16

```

268 AutoEncoders

269 Over the last decade, neural networks have gained significant popularity in all applications of
 270 science and engineering [52, 53]. Advances in computational power and data availability make
 271 neural networks candidate methods for ~~all~~^A types of complex problems including computer vision.
 272 In general, neural networks can be posed as an optimization function over a functional composition
 273 such that,

$$\operatorname{argmin}_{A_j} f_M(A_m, \dots, f_2(A_2, f_1(A_1, x)) \dots) + \lambda g(A_j), \quad (21)$$

274 where A_k represents the matrix of weights ~~associated~~ between the layers k and $k + 1$ of the
 275 network, f is a nonlinear operator, and $g(\cdot)$ and λ are a regularization function and weight,
 276 respectively. The optimization problem quickly becomes a severely ill-posed problem due to the
 277 large numbers of parameters, A_k , and is typically solved by stochastic gradient descent algorithms
 278 and backpropagation [54].

279 Convolutional Neural Networks (CNNs) are a specialized type of neural network architecture
 280 designed for processing data that has a known grid-like topology, such as images [55]. Furthermore,
 281 they provide inherent regularization properties through the extraction of smaller pixel subsets
 282 and simpler patterns from images. The convolution operator extracts features from overlapping
 283 receptive fields over a hierarchy, such as the process of human vision [56]. This property exploits
 284 locally correlated patterns while minimizing the correlations at large distances. The convolutional
 285 filters have properties of translational equivariance and local shift invariance, where the learned
 286 weights in the filters are optimized to extract dominant patterns and structures in the data.

287 Convolutional AutoEncoders (AEs) are a special architecture of neural networks used for image
 288 compression, denoising, and translation [57, 58]. The main idea behind AEs is to compress the
 289 original data matrix, X , into a latent representation of reduced dimensions, z , through an *encoder*
 290 portion of the architecture, and then use a mirror image of the Encoder, namely the *decoder*, to
 291 reconstruct the data matrix, X' , such that,

$$X \approx X' = dec(enc(X)) = dec(z). \quad (22)$$

292 The Encoder and Decoder portions of the network are composed of multiple convolutional layers,
 293 where each layer includes a pooling (~~decrease dimensions~~) or upsampling (~~increase dimensions~~)
 294 operator for the case of the Encoder and Decoder, respectively. The latent representation, also
 295 known as latent space, z , must be able to capture the majority of the patterns and structures in
 296 the data while maximally reducing the dimensions.

297 One of the main issues when designed^A AEs for dimensionality reduction is the vast number
 298 of hyperparameters [59]. The number and size of each hidden layer, convolutional filter (kernel)
 299 size, stride, padding, pooling and upsampling rates, normalization, nonlinear activation function,
 300 optimizer, learning rate, number of training epochs, loss function, and other hyperparameters
 301 must be carefully considered and tuned to obtain the best possible AE for a given dataset.

302 **Example**

303 Given the architectural complexity of designing neural networks for dimensionality reduction, we
 304 will focus on a simple convolutional AutoEncoder architecture to demonstrate the use ease on
 305 our geologic uncertainty model. The first step is to expand the dimensions of our dataset such
 306 that $X \in \mathbb{R}^{500 \times 1 \times 128 \times 128}$, where the new dimension represents the channel dimensions. We design
 307 an AE with three layers in the Encoder, and three mirroring layers in the Decoder, each with a
 308 convolution, batch normalization, and rectified linear unit (ReLU) activation. In the Encoder,
 309 maximum pooling is used to decrease the dimensions of the data, such that,

$$X_j \in \mathbb{R}^{b \times c_j \times \frac{n_x^j}{2} \times \frac{n_y^j}{2}} \quad (23)$$

310 where b represents the batch size and c represents the number of channels. On the other hand,
 311 the Decoder uses an upsampling operator to increase the dimensions of the data such that,

$$X'_j \in \mathbb{R}^{b \times c_j \times 2n_x^j \times 2n_y^j}. \quad (24)$$

312 The number of channels for each of the three Encoder and Decoder layers is selected as 16, 64,
 313 and 256, respectively, meaning that the latent space is given by,

$$z \in \mathbb{R}^{b \times 256 \times 16 \times 16}. \quad (25)$$

314 We use the Adam optimizer with learning rate 0.001 and MSE loss function for 200 epochs, and
 315 train the model using an NVIDIA RTX 6000 Ada GPU. The total number of trainable parameters in the model is 314,883, and the reconstruction metrics are $R^2 = 92.35$, $MSE = 0.029$, and
 316 $SSIM = 89.75$. Figure 19 shows the loss function per epoch, demonstrating significant stability and minimal overfitting between the training and validation sets. Finally, Figure 20 shows
 317 the reconstructed images in the geologic uncertainty ensemble using our AE. We observe that
 318 the convolutional AE smooths the data, which is a common concern when using this architecture.
 319 However, all large-scale features and the majority of the fine-scale details are preserved and
 320 reconstructed using this architecture.

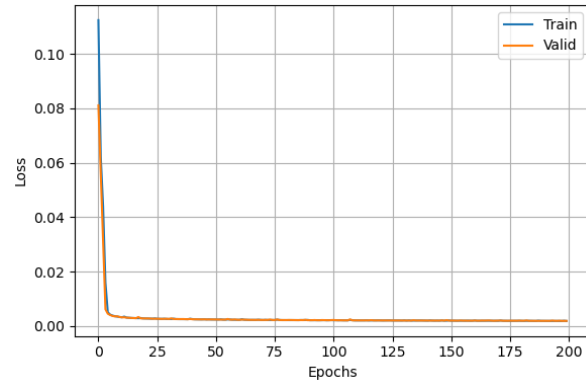


Figure 19: Loss function versus number of epochs.

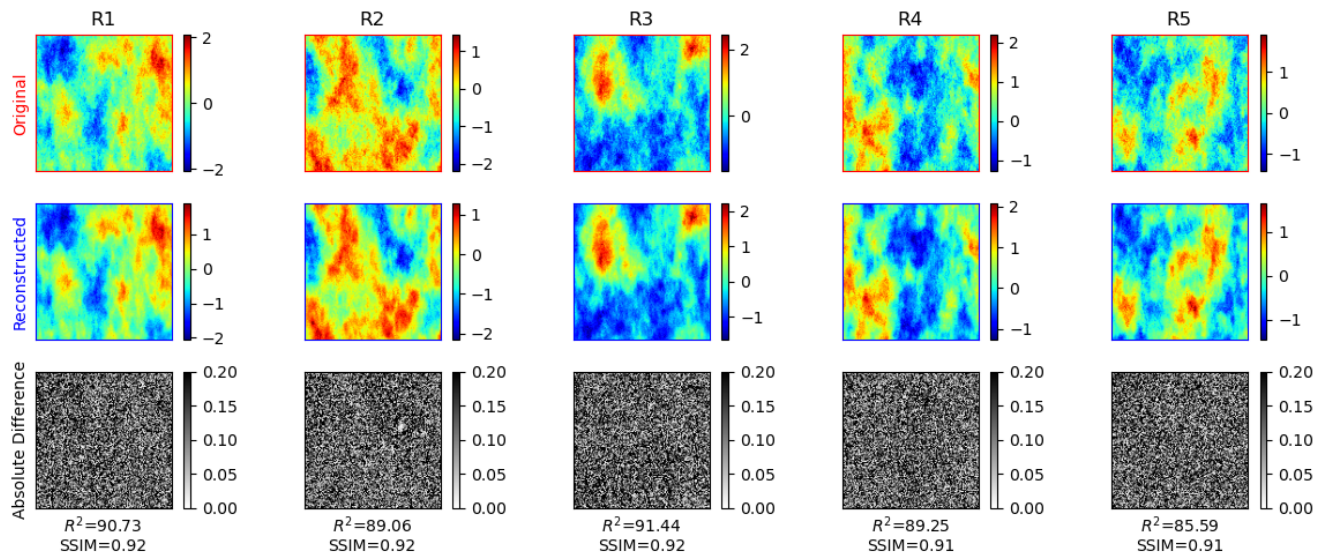


Figure 20: Reconstructed image using latent dimension 256 in the AutoEncoder.

```

1 import numpy as np
2 import torch
3 import torch.nn as nn
4 import torch.optim as optim
5 import torch.nn.functional as F
6 from torch.utils.data import DataLoader, TensorDataset
7 from torch.utils.data import random_split
8 from sklearn.preprocessing import MinMaxScaler
9
10
11 df_perm = np.load('data/data_500_128x128.npy')
12 df_perm_f = np.reshape(df_perm, (df_perm.shape[0], -1))
13
14 class AutoEncoder(nn.Module):
15     def __init__(self, layers=[4, 16, 64]):
16         super(AutoEncoder, self).__init__()
17         self.encoder = nn.Sequential(
18             self.conv_block(1, layers[0]),
19             self.conv_block(layers[0], layers[1]),
20             self.conv_block(layers[1], layers[2]),
21         )
# array operations
# deep learning library
# neural network operations
# neural network optimizer
# functional layers
# tensor data opearitions
# random train-test split
# data preprocessing
# (500, 128, 128)
# (500, 16384)
# AutoEncoder architecture class
# size of 3 hidden layers
# ENCODER
# first encoding layer
# second encoding layer
# third encoding layer

```

```

22         self.decoder = nn.Sequential(                               # DECODER
23             self.deconv_block(layers[2], layers[1]),                # first decoding layer
24             self.deconv_block(layers[1], layers[0]),                # second decoding layer
25             self.deconv_block(layers[0], 1),                         # third decoding layer
26         )
27
28     def conv_block(self, ic, oc):                                # architecture of encoding layer
29         return nn.Sequential(
30             nn.Conv2d(ic, oc, kernel_size=3, padding=1),          # convolution
31             nn.BatchNorm2d(out_channels),                         # batch normalization
32             nn.ReLU(),                                         # activation
33             nn.MaxPool2d(kernel_size=2, stride=2)                 # pooling
34         )
35
36     def deconv_block(self, ic, oc):                                # architecture of decoding layer
37         return nn.Sequential(
38             nn.Upsample(scale_factor=2),                           # upsampling
39             nn.Conv2d(ic, oc, kernel_size=3, padding=1),          # convolution
40             nn.BatchNorm2d(oc),                                 # batch normalization
41             nn.ReLU()                                           # activation
42         )
43
44     def forward(self, x):                                       # AutoEncoder
45         z = self.encoder(x)                                    # Encoder
46         y = self.decoder(z)                                  # Decoder
47         return y
48
49
50 scaler = MinMaxScaler()                                     # initialize data scaler
51 scaler.fit(df_perm_f)                                      # fit data scaler
52 XX = scaler.transform(df_perm_f).reshape(df_perm.shape)    # normalize data
53 X_dataset = torch.tensor(np.expand_dims(XX,1), dtype=torch.float32) # tensor dataset
54 X_train, X_valid = random_split(X_dataset, [450, 50])      # train-valid split
55 trainloader = DataLoader(X_train, batch_size=16, shuffle=True) # training data loader
56 validloader = DataLoader(X_valid, batch_size=16, shuffle=False) # validation data loader
57
58 device = torch.device("cuda" if torch.cuda.is_available() else "cpu") # use GPU for training
59 model = AutoEncoder(layers=[16, 64, 256]).to(device)               # initialize NN
60 optimizer = optim.Adam(params=model.parameters(), lr=1e-3)        # initialize optimizer
61 criterion = nn.MSELoss().to(device)                                # initialize loss

```

```

62
63 epochs = 200                                # define number of training epochs
64 train_loss, valid_loss = [], []                # initialize train and valid losses
65 for epoch in range(epochs):                   # begin training loop
66     # training
67     epoch_train_loss = []                      # reset epoch loss - train
68     for i, x in enumerate(trainloader):         # send batch to GPU
69         x = x.to(device)                        # reset gradients
70         optimizer.zero_grad()                  # forward pass
71         y = model(x)                          # calculate loss
72         loss = criterion(y, x)                # backward pass
73         loss.backward()                       # calculate gradients
74         optimizer.step()                     # append epoch loss
75         epoch_train_loss.append(loss.item()) # appen total loss
76     train_loss.append(np.mean(epoch_train_loss)) # validation
77     # validation
78     model.eval()                            # freeze model
79     epoch_valid_loss = []                   # reset epoch loss - valid
80     with torch.no_grad():
81         for i, x in enumerate(validloader):    # send batch to GPU
82             x = x.to(device)                  # forward pass
83             y = model(x)                    # calculate loss
84             loss = criterion(y, x)          # append epoch loss
85             epoch_valid_loss.append(loss.item())
86             valid_loss.append(np.mean(epoch_valid_loss)) # append total loss
87
88 # Obtain final predictions for dataset and back-normalize
89 pred = model(X_dataset.to(device)).cpu().detach().numpy().squeeze()
90 xhat = scaler.inverse_transform(pred.reshape(df_perm_f.shape)).reshape(df_perm.shape)
91

```

323 Conclusions

324 Dimensionality reduction techniques serve as powerful algorithms to project high-dimensional,
325 complex datasets into lower dimensionality while attempting to minimize the loss of information by
326 extracting relevant patterns and feature in the data. Furthermore, Encoder-Decoder architectures
327 provide powerful algorithms to compress data into a latent space and a back-projection to the
328 original data space. The latent representation, z , is designed to contain the most salient features
329 of the data, and can be used as a proxy for complex and time-consuming routines such as reservoir
330 simulation and history matching in the case of subsurface energy resource engineering.

331 Several dimensionality reduction algorithms were shown, namely singular value decomposition,
332 principal component analysis, discrete wavelet transform, dictionary learning, and deep learning
333 AutoEncoders. However, a much long list of dimensionality reduction algorithms exists and can
334 be useful for different types of datasets and applications. Table shows a comparison of the
335 different dimensionality reduction techniques applied to the geologic uncertainty model dataset
336 in terms of reconstruction accuracy and computational costs. Ultimately, the goal is to obtain a
337 compressed representation of the data that can be used to accelerate expensive computations, and
338 the user must carefully select and design the dimensionality reduction algorithm according to the
339 data needs. The tradeoff between compression and reconstruction accuracy is typically the main
340 concern, as perfectly lossless compression is hard to obtain, and most engineering applications can
341 benefit from slightly lossy compression at the benefit of significant computational acceleration.

	20% CR	50% CR	80% CR	95% CR	Time [s]
SVD	11	83	288	441	21.1
PCA	2	8	36	234	2.6
DWT	7	30	60	125	1.3
DL	16	191	426	491	94.6

Table 1: Latent space dimension based on reconstruction accuracy. Four different dimensionality reduction techniques (SVD, PCA, DWT, DL) are compared based on different compression ratios (*coefficients retained / total number of features*) and their average CPU time required for compression and reconstruction.

342 Code Availability

343 The code is publicly available on the author's GitHub repository:
344 <https://github.com/misaelmmorales/Dimensionality-Reduction>

³⁴⁵ **Acknowledgments**

³⁴⁶ The authors thank the Formation Evaluation (FE) and Digital Reservoir Characterization Tech-
³⁴⁷ nology (DIRECT) Industry Affiliate Programs at the University of Texas at Austin for supporting
³⁴⁸ this work.

³⁴⁹ **Declaration of competing interest**

³⁵⁰ The authors declare that they have no known competing financial interests or personal relation-
³⁵¹ ships that could have appeared to influence the work reported in this paper.

References

- [1] Mehdi Mohammadpoor and Farshid Torabi. Big data analytics in oil and gas industry: An emerging trend. *Petroleum*, 6(4):321–328, 2020.
- [2] Abdeldjalil Latrach, Mohamed L Malki, Misael Morales, Mohamed Mehana, and Minou Rabiei. A critical review of physics-informed machine learning applications in subsurface energy systems. *Geoenergy Science and Engineering*, page 212938, 2024.
- [3] Oriyomi Raheem, Wen Pan, Misael M Morales, and Carlos Torres-Verdín. Best practices in automatic permeability estimation: machine-learning methods vs. conventional petrophysical models. *Petrophysics-The SPWLA Journal of Formation Evaluation and Reservoir Description*, 65(05):789–812, 2024.
- [4] Shaowen Mao, Bailian Chen, Mohamed Malki, Fangxuan Chen, Misael Morales, Zhiwei Ma, and Mohamed Mehana. Efficient prediction of hydrogen storage performance in depleted gas reservoirs using machine learning. *Applied Energy*, 361:122914, 2024.
- [5] Misael M Morales, Oriyomi Raheem, Carlos Torres-Verdín, Michael Pyrcz, Murray Christie, and Vladimir Rabinovich. Automatic rock classification from core data to well logs: Using machine learning to accelerate potential co₂ storage site characterization. In *Fourth International Meeting for Applied Geoscience & Energy*, pages 632–636. Society of Exploration Geophysicists and American Association of Petroleum . . . , 2024.
- [6] Misael M Morales, Carlos Torres-Verdín, Michael Pyrcz, Murray Christie, and Vladimir Rabinovich. Automatic well-log baseline correction via deep learning for rapid screening of potential co₂ storage sites. In *SEG International Exposition and Annual Meeting*, pages SEG–2024. SEG, 2024.

- [7] K. Rashid, W. Bailey, B. Couët, and D. Wilkinson. An efficient procedure for expensive reservoir-simulation optimization under uncertainty. *SPE Economics and Management*, 5(4):21–33, 2013. doi: 10.2118/167261-PA.
- [8] Javier E. Santos, Bernard Chang, Alex Gigliotti, Eric Guiltinan, Mohamed Mehana, Arvind Mohan, James McClure, Qinjun Kang, Hari Viswanathan, Nicholas Lubbers, Masa Prodanovic, and Michael Pyrcz. Learning from a big dataset of digital rock simulations. In *AGU Fall Meeting Abstracts*, volume 2021, pages H25O–1207, December 2021.
- [9] Shaowen Mao, Bailian Chen, Misael Morales, Mohamed Malki, and Mohamed Mehana. Cushion gas effects on hydrogen storage in porous rocks: Insights from reservoir simulation and deep learning. *International Journal of Hydrogen Energy*, 68:1033–1047, 2024.
- [10] Zeeshan Tariq, Murtada Saleh Aljawad, Amjad Hasan, Mobeen Murtaza, Emad Mohammed, Ammar El-Husseiny, Sulaiman A Alarifi, Mohamed Mahmoud, and Abdulazeez Abdulraheem. A systematic review of data science and machine learning applications to the oil and gas industry. *Journal of Petroleum Exploration and Production Technology*, pages 1–36, 2021.
- [11] Anirbid Sircar, Kriti Yadav, Kamakshi Rayavarapu, Namrata Bist, and Hemangi Oza. Application of machine learning and artificial intelligence in oil and gas industry. *Petroleum Research*, 6(4):379–391, 2021.
- [12] Jie Cai, Jiawei Luo, Shulin Wang, and Sheng Yang. Feature selection in machine learning: A new perspective. *Neurocomputing*, 300:70–79, 2018.
- [13] Alice Zheng and Amanda Casari. *Feature engineering for machine learning: principles and techniques for data scientists.* ” O'Reilly Media, Inc.”, 2018.
- [14] Siddharth Misra, Hao Li, and Jiabo He. *Machine learning for subsurface characterization.* Gulf Professional Publishing, 2019.
- [15] Shuvajit Bhattacharya. *A primer on machine learning in subsurface geosciences*, volume 1. Springer, 2021.
- [16] Misael M Morales, Ali Eghbali, Oriyomi Raheem, Michael J Pyrcz, and Carlos Torres-Verdín. Anisotropic resistivity estimation and uncertainty quantification from borehole triaxial electromagnetic induction measurements: Gradient-based inversion and physics-informed neural network. *Computers & Geosciences*, 196:105786, 2025.
- [17] Misael M Morales, Carlos Torres-Verdín, and Michael J Pyrcz. Stochastic pix2vid: A new spatiotemporal deep learning method for image-to-video synthesis in geologic co 2 storage prediction. *Computational Geosciences*, pages 1–22, 2024.

- [18] Su Jiang and Louis J Durlofsky. Use of multifidelity training data and transfer learning for efficient construction of subsurface flow surrogate models. *Journal of Computational Physics*, 474:111800, 2023.
- [19] Ademide O Mabadeje and Michael J Pyrcz. Evaluating the stability of deep learning latent feature spaces. *arXiv preprint arXiv:2402.11404*, 2024.
- [20] Ademide O Mabadeje and Michael J Pyrcz. Rigid transformations for stabilized lower dimensional space to support subsurface uncertainty quantification and interpretation. *Computational Geosciences*, pages 1–21, 2024.
- [21] Misael M Morales, Mohamed Mehana, Carlos Torres-Verdín, Michael J Pyrcz, and Bailian Chen. Optimal monitoring design for uncertainty quantification during geologic co₂ sequestration: A machine learning approach. *Geoenergy Science and Engineering*, 244:213402, 2025.
- [22] Bailian Chen, Misael M Morales, Zhiwei Ma, Qinjun Kang, and Rajesh J Pawar. Assimilation of geophysics-derived spatial data for model calibration in geologic co₂ sequestration. *SPE Journal*, pages 1–10, 2024.
- [23] Michael J Pyrcz and Clayton V Deutsch. *Geostatistical reservoir modeling*. Oxford University Press, USA, 2014.
- [24] Michael J Pyrcz. *Applied Geostatistics in Python: a Hands-on guide with GeostatsPy*. <https://geostatsguy.github.io/GeostatsPyDemosBook>, 2024.
- [25] N Remy. *Applied geostatistics with SGEMS: A user's guide*. Cambridge University Press, 2009.
- [26] Virginia Klema and Alan Laub. The singular value decomposition: Its computation and some applications. *IEEE Transactions on automatic control*, 25(2):164–176, 1980.
- [27] Gilbert W Stewart. On the early history of the singular value decomposition. *SIAM review*, 35(4):551–566, 1993.
- [28] Michael E Wall, Andreas Rechtsteiner, and Luis M Rocha. Singular value decomposition and principal component analysis. In *A practical approach to microarray data analysis*, pages 91–109. Springer, 2003.
- [29] Kirk Baker. Singular value decomposition tutorial. *The Ohio State University*, 24:22, 2005.
- [30] Steven L Brunton and J Nathan Kutz. *Data-driven science and engineering: Machine learning, dynamical systems, and control*. Cambridge University Press, 2022.
- [31] Sardar Afra and Eduardo Gildin. Tensor based geology preserving reservoir parameterization with higher order singular value decomposition (hosvd). *Computers & geosciences*, 94:110–120, 2016.

- [32] Per Christian Hansen. Truncated singular value decomposition solutions to discrete ill-posed problems with ill-determined numerical rank. *SIAM Journal on Scientific and Statistical Computing*, 11(3):503–518, 1990.
- [33] Pallav Sarma, Louis J Durlofsky, Khalid Aziz, and Wen H Chen. A new approach to automatic history matching using kernel pca. In *SPE Reservoir Simulation Conference?*, pages SPE–106176. SPE, 2007.
- [34] Hai X Vo and Louis J Durlofsky. A new differentiable parameterization based on principal component analysis for the low-dimensional representation of complex geological models. *Mathematical Geosciences*, 46:775–813, 2014.
- [35] Michael J Pyrcz. *Applied Machine Learning in Python: a Hands-on Guide with Code*. <https://geostatsguy.github.io/MachineLearningDemosBook>, 2024.
- [36] Ian T Jolliffe and Jorge Cadima. Principal component analysis: a review and recent developments. *Philosophical transactions of the royal society A: Mathematical, Physical and Engineering Sciences*, 374(2065):20150202, 2016.
- [37] Hervé Abdi and Lynne J Williams. Principal component analysis. *Wiley interdisciplinary reviews: computational statistics*, 2(4):433–459, 2010.
- [38] KH Esbensen and Paul Geladi. 2.02-principal component analysis: Concept, geometrical interpretation, mathematical background, algorithms, history, practice. In *Comprehensive chemometrics: Chemical and biochemical data analysis*, volume 2. 2020.
- [39] Pierre Duhamel and Martin Vetterli. Fast fourier transforms: a tutorial review and a state of the art. *Signal processing*, 19(4):259–299, 1990.
- [40] Zongyi Li, Nikola Kovachki, Kamyar Azizzadenesheli, Burigede Liu, Kaushik Bhattacharya, Andrew Stuart, and Anima Anandkumar. Fourier neural operator for parametric partial differential equations. *arXiv preprint arXiv:2010.08895*, 2020.
- [41] Iorio Júnior Iorio Jr and Valéria de Magalhães Iorio. *Fourier analysis and partial differential equations*. Number 70. Cambridge University Press, 2001.
- [42] James W Cooley, Peter AW Lewis, and Peter D Welch. The fast fourier transform and its applications. *IEEE Transactions on Education*, 12(1):27–34, 1969.
- [43] Henri J Nussbaumer and Henri J Nussbaumer. *The fast Fourier transform*. Springer, 1982.
- [44] G Susrutha, K Mallikarjun, M Ajay Kumar, and M Ashok. Analysis on fft and dwt transformations in image processing. In *2019 International Conference on Emerging Trends in Science and Engineering (ICESE)*, volume 1, pages 1–4. IEEE, 2019.

- [45] Christopher E Heil and David F Walnut. Continuous and discrete wavelet transforms. *SIAM review*, 31(4):628–666, 1989.
- [46] Tim Edwards. Discrete wavelet transforms: Theory and implementation. *Universidad de*, 1991: 28–35, 1991.
- [47] Gheyath Othman and Diyar Qader Zeebaree. The applications of discrete wavelet transform in image processing: A review. *Journal of Soft Computing and Data Mining*, 1(2):31–43, 2020.
- [48] Ivana Tošić and Pascal Frossard. Dictionary learning. *IEEE Signal Processing Magazine*, 28(2): 27–38, 2011.
- [49] Julien Mairal, Jean Ponce, Guillermo Sapiro, Andrew Zisserman, and Francis Bach. Supervised dictionary learning. *Advances in neural information processing systems*, 21, 2008.
- [50] Kenneth Kreutz-Delgado, Joseph F Murray, Bhaskar D Rao, Kjersti Engan, Te-Won Lee, and Terrence J Sejnowski. Dictionary learning algorithms for sparse representation. *Neural computation*, 15(2):349–396, 2003.
- [51] Entao Liu and Behnam Jafarpour. Learning sparse geologic dictionaries from low-rank representations of facies connectivity for flow model calibration. *Water Resources Research*, 49(10): 7088–7101, 2013.
- [52] Ian Goodfellow. *Deep learning*, volume 196. MIT press, 2016.
- [53] Wengang Zhang, Xin Gu, Libin Tang, Yueping Yin, Dongsheng Liu, and Yanmei Zhang. Application of machine learning, deep learning and optimization algorithms in geoengineering and geoscience: Comprehensive review and future challenge. *Gondwana Research*, 109:1–17, 2022.
- [54] Léon Bottou et al. Stochastic gradient learning in neural networks. *Proceedings of Neuro-Nîmes*, 91(8):12, 1991.
- [55] Zewen Li, Fan Liu, Wenjie Yang, Shouheng Peng, and Jun Zhou. A survey of convolutional neural networks: analysis, applications, and prospects. *IEEE transactions on neural networks and learning systems*, 33(12):6999–7019, 2021.
- [56] Wenjie Luo, Yujia Li, Raquel Urtasun, and Richard Zemel. Understanding the effective receptive field in deep convolutional neural networks. *Advances in neural information processing systems*, 29, 2016.
- [57] Jinsheng Jiang, Haoran Ren, and Meng Zhang. A convolutional autoencoder method for simultaneous seismic data reconstruction and denoising. *IEEE geoscience and remote sensing letters*, 19: 1–5, 2021.

- [58] Ming-Yu Liu, Thomas Breuel, and Jan Kautz. Unsupervised image-to-image translation networks. *Advances in neural information processing systems*, 30, 2017.
- [59] Frank Hutter, Jörg Lücke, and Lars Schmidt-Thieme. Beyond manual tuning of hyperparameters. *KI-Künstliche Intelligenz*, 29:329–337, 2015.